Dye-Doped Silica Nanoparticles for Enhanced ECL-Based Immunoassay Analytical Performance

Dye-doped silica nanoparticles for enhanced ECL-based immunoassay analytical performance

Alessandra Zanut,[a,b,†] Francesco Palomba, [a,c,†] Matilde Rossi Scota,[a] Sara Rebeccani,[a] Massimo Marcaccio,[a] Damiano Genovese,[a] Enrico Rampazzo,[a] Giovanni Valenti,[a] Francesco Paolucci,[a] Luca Prodi* [a]

[a] *Department of Chemistry "Giacomo Ciamician", University of Bologna, Bologna (Italy) Email: luca.prodi@unibo.it*

[b] *Current address: Dr. F. Palomba, Department of Biomedical Engineering University of California Irvine, Irvine, CA, 92697, USA.*

[c] *Current address: Dr. A. Zanut, Tandon School of Engineering, New York University, Brooklyn, NY, 11201 USA.*

[†] *These authors contributed equally to this work.*

Abstract: The combination of highly sensitive techniques such as Electrochemiluminescence (ECL) with nanotechnology sparkled new analytical applications in particular for immunoassay-based detection systems. In this context, nanomaterials, in particular dye-doped silica nanoparticles (DDSNPs) are of particular interest, since they can offer several advantages in terms of sensitivity and performance. In this work we synthesized two sets of monodispersed and biotinylated $[Ru(bpy)_3]^{2+}$-doped silica nanoparticles, named bio-Triton@RuNP and bio-Igepal@RuNP, obtained following the reverse microemulsion method using two different types of nonionic surfactants. Controlling the synthetic procedures, we were able to obtain nanoparticles (NPs) offering highly intense signal, using tri-*n*-propylamine (TPrA) as coreactant, with bio-Triton@RuNps being more efficient than bio-Igepal@RuNP. Interestingly, although only a small portion of the 4800 complexes contained in each NP was involved in signal generation, when used in ECL analytical mode Bio-Triton@RuNPs reveal ECL intensity 8.5-fold higher compared to a system mimicking a commercial ECL-based immunoassay system. In addition, these NPs showed an improved ECL stability because of the silica matrix, increasing even more their potential performance. Overall, our results support the application of these NPs in ECL microscopy techniques and suggest a possible further signal increase achievable acting on the synthetic procedure, opening new promising paths towards more sensitive ECL-based immunoassay, with applications for biosensing and for point-of-care devices.

The quantification of diagnostic markers, or biomarkers, is one of the most stimulating and intriguing fields of research due to its enormous impact in the early diagnosis from basic research to clinical applications. However, the detection of very low amounts of these molecules with simple and accurate methods is still an open issue. In this context, electrochemiluminescence (ECL) appears to be a leading transduction technique. ECL is based on the electrochemical generation of species that undergo high-energy electron transfer reactions to form light-emitting excited states.[1][2][3] The combination of electrochemical and spectroscopic methods makes ECL a powerful analytical technique,[4] whose main advantageous feature is the remarkable signal-to-noise ratio due to the absence of a light source for excited states generation. ECL boasts also excellent spatial and temporal control with the possibility of performing rapid measurements on small sample volumes. High sensitivity, negligible background, high spatial and temporal control, and the possibility to be performed in aqueous solutions brought important development to the use of ECL as a unique analytical technique. Indeed, ECL has been used for immunoassay and ultrasensitive detection of a wide range of analytes in different fields like medical diagnostics, environmental analysis, and

(bio)sensors fabrication[5][4][6][7][8] The subsequent application of ECL principles in microscopy allowed new frontiers and new applications in particular for multiplexing analysis,[9][10][11] making the investigation of the ECL mechanisms possible at nanoscale level, especially for sensor application and for biological characterizations. For these reasons, ECL microscopy is a very promising technique for the surface-confined mapping and quantification of several extremely diluted analytes [12][13][14][15][16][17][18][19].

The most used strategy to generate ECL in an aqueous environment is based on the so-called *oxidative-reduction* co-reactant mechanism where tri-*n*-propylamine (TPrA) is used as sacrificial co-reactant and tris(2,2'-bipyridine)ruthenium(II) ($[Ru(bpy)_3]^{2+}$) as luminophore[20–22], allowing a tremendous number of applications[23]. This strategy is employed also in commercialized ECL-based immunoassays developed by Roche Diagnostics (Elecsys®)[24] and Meso Scale Diagnostics.[25]

Chasing an ever-increasing sensitivity, many researchers tried to combine ECL with nanomaterials, such as nanoparticles, using them as dyes or co-reactants [26–31]. In particular, dye-doped silica nanoparticles (DDSNPs) have proved to be a very interesting option as ECL dyes, due to their several advantages such as (i) an enhanced signal intensity (up to a potential thousand-fold increase) thanks to a large number of inner active dyes[32,33], (ii) a simple and versatile synthetic schemes for their preparation, which typically afford high colloidal stability in water, and (iii) an easy bioconjugation. [34][35]

However, we recently revealed some limitations on the use of DDSNPs that strongly depend on the synthetic strategy adopted [26]. One of the major issues, in common with fluorescent particles, is the potential difficulty to dope the NPs with organic or inorganic dyes mainly due to solubility issue and/or electrostatic interactions which generally hampers the use of negatively charged species. Nevertheless, this issue can be conveniently addressed with a proper control of the synthetic procedures and of the physical chemical properties of silica NPs.[36,37]

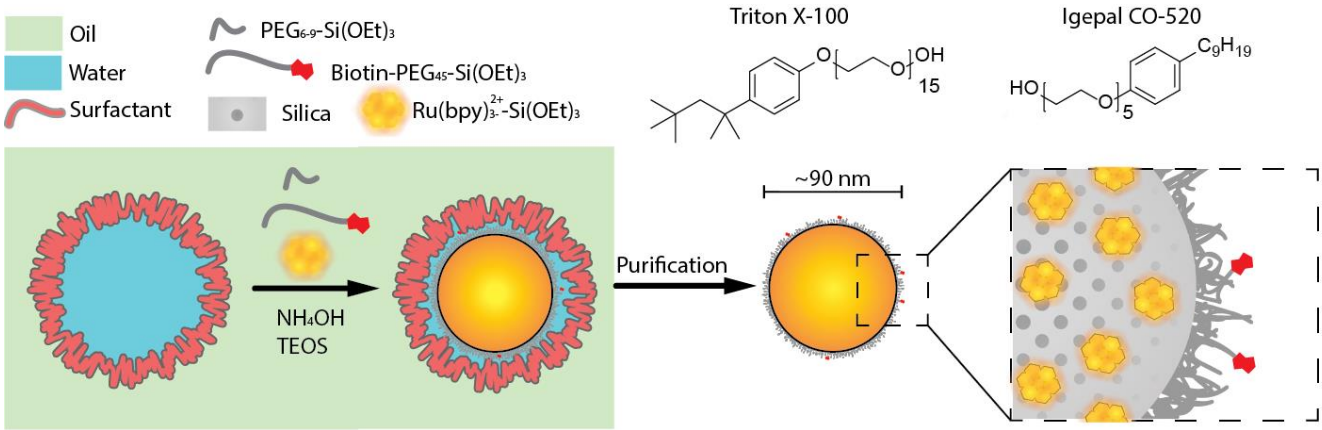

Figure 1. Schematic representation of the Reverse Micro Emulsion synthesis of $[Ru(bpy)_3]^{2+}$doped silica nanoparticles. The synthesis starts with the preparation of the water in oil emulsion stabilized with non-ionic surfactants (Triton X-100 or Igepal CO-520), then upon the addition of $[Ru(bpy)_3]^{2+}$ triethoxy silane derivative ($Ru(bpy)_3^{2+}$-$Si(OEt)_3$), tetraethoxyorthosilicate (TEOS) and, ammonium hydroxide (NH_4OH) the dye-doped silica core is formed. The NPs are then coated with antifouling agent polyethylenglycol triethoxy silane derivative ($PEG_{6-9}Si(OEt)_3$) and with biotin tagged polythylenglycol triethoxysilane derivative(Biotin-PEG_{45}-$Si(OEt)_3$). The synthesis ends with the purification of the NPs from the surfactant and the oil phase.

Another potential problem related to the use of DDSNPs is that the process leading to the formation of the emitting excited state in ECL is much more complex than in photo-luminescence, in which the

exciting light easily crosses the transparent silica matrix without its involvement in any quenching (energy- or electron-transfer) process. Particularly in case of DDSNPs, the generation of the ECL signal typically starts from the oxidation of the co-reactant (whose choice is thus of particular importance) at the electrode surface; the oxidized species and their products, which are radical species with a limited lifetime, has to diffuse to quickly reach the ECL probes inside the silica matrix, finally generating the emitting excited state.

This implies that, to increase the sensitivity offered by DDSNPs, their dimension should be optimized considering that the amount of ECL-active species is strictly connected to the NP volume. At the same time, in excessively large particles, this advantage is counterbalanced by the fact that too many probes are not reachable by the diffusing radical species.[32] Moreover, the nature of NP surface, including its shell, should be engineered in order to make the NPs colloidally stable in water and endowed with groups suitable for proper derivatization but at the same time to allow the fast diffusion of the radical; in particular thin shells with an overall negative ζ potential are expected to give the highest signals [38]. Finally, porosity is also expected to play an important and favourable role, thus the synthetic procedure should consider this effect.

Among all the insights we obtained so far on the ECL generation using DDSNPs, the majority of them were obtained with PluS NPs,[38,33] synthesised with a direct micelle-assisted method taking profit of the Pluronic-F127 surfactant. To further push the signal intensity, in this work we present silica NPs synthesized with a reverse microemulsion method, that allows to obtain a suspension of monodispersed NPs with greater flexibility in terms of particle size and surface properties and with different surface functionalization, through an excellent control on the synthetic parameters.[39,40] In particular, we obtained here (synthetic scheme in Figure 1) two sets of monodispersed $Ru(bpy)_3^{2+}$-doped silica NPs, namely bio-Triton@RuNP and bio-Igepal@RuNP, using two different types of nonionic surfactants (TritonX-100 and Igepal CO-520), $[Ru(bpy)_3]^{2+}$-$Si(OEt)_3$ derivative as a dye and biotinylated polyethylene glycol-$Si(OEt)_3$ as biorecognition unit. The core (∼ 90nm) and hydrodynamic (d_H ∼ 150nm) diameters – determined by TEM and DLS respectively (see figures 2A and 2B) – of bio-Triton@RuNP and bio-Igepal@RuNP are reported in Table 1. It can be noted that they are almost independent on the surfactant used. (see figure S1).

The absorption and emission spectra, reported in Figure 2, show that the peak shape and position of the two sets of NPs are similar to each other, as well as to $[Ru(bpy)_3]^{2+}$ in water solution (grey line), since silica matrix is not dramatically perturbing the electronic ground state conditions. The phosphorescence quantum yield Φ and the average lifetime of the dye in bio-Triton@RuNPs (Φ_{PL} = 0.080, τ ~ 790 ns) show about three-fold increase respect to the free $[Ru(bpy)_3]^{2+}$ dye (Φ_{PL} = 0.028, τ = 334 ns) in aerated water solutions, while a lower increase has been observed for bio-Igepal@RuNPs (Φ_{PL} = 0.050, τ ~ 618 ns). The increase of the phosphorescence quantum yield and the lengthening of the excited state lifetime can be attributed to the reduced diffusion rate of molecular oxygen in the silica matrix[41], that depends on the synthetic procedure.

By assuming that the absorption coefficient of the $[Ru(bpy)_3]^{2+}$ complexes is not significantly altered because of their insertion inside the silica matrix, we were able to estimate (for further details, see SI) that each NP includes an average of 3200 and 4800 ruthenium complexes for bio-Igepal@RuNP and bio-Triton@RuNP, respectively, despite the same initial doping level (2%). It is noteworthy that, although the number of dyes was higher in bio-Triton@RuNP, in these NPs the ζ-potential remained very close to 0 mV unlike previous results with PluS NPs[33,38], while a slightly positive value was found for bio-Igepal@RuNP.

Table 1. % mol of dyes vs mol of TEOS and number of dyes value of bio-Triton@RuNP and bio-Igepal@RuNP. Hydrodynamic diameter, core diameter, polidispersion index (PDI), ζ-potential measured at pH 6.7,

sample	% mol dye/mol TEOS	no. dye/NP	d_H ± SD [nm]	d_H ± SD [nm]	PDI	ζ potential [mV]
bio-Triton@RuNP	2	4800	90 ± 10	145 ± 5	0.10	1.3+0.6
bio-Igepal@RuNP	2	3200	85 ± 20	150 ± 10	0.15	6.8±1.5

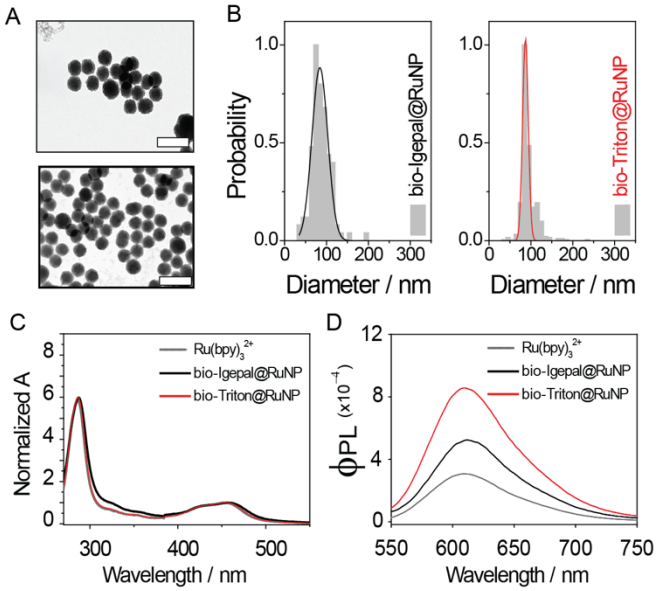

Figure 2. (A) TEM Images of Silica NPs top: bio-Igepal@RuNP, bottom: bio-Triton@RuNP. (scale bar 200 nm). (B) Silica core diameters distributions computed by TEM. left: bio-Igepal@RuNP and right bio-Triton@RuNP. (C-D) Normalized absorption and phosphorescence quantum yield of bio-Igepal@RuNP (black line), bio-Triton@RuNP (red line) and $[Ru(bpy)_3]^{2+}$ (grey line) in water as reference for comparison.

To test the ECL performances of the two sets of NPs, cyclic voltammetry (CV) was performed on 1nM of NPs using TPrA (180 mM) as sacrificial co-reactant and the ECL intensity was acquired from a photomultiplier tube applying a bias of 750 V. In Figure 3, the registered ECL intensity was plotted against the potential scanned between 0 V and +1.6V. The general mechanism active in this condition for the ECL generation is based on the so-called *oxidative-reduction* co-reactant mechanism schematize in figure 3A and with the following equation:

$$TPrA - e^- \leftrightarrows TPrA^{\bullet+} \quad (1)$$

$$TPrA^{\bullet+} \leftrightarrows TPrA^{\bullet} + H^+ \quad (2)$$

$$TPrA^{\bullet} + \text{bio-Triton@RuNps} \leftrightarrows P1 + \text{bio-Triton@}Ru^{-}\text{Nps} \quad (3)$$

$$TPrA^{\bullet+} + \text{bio-Triton@}Ru^{-}\text{Nps} \leftrightarrows TPrA + \text{bio-Triton@}Ru^{*}\text{Nps} \quad (4)$$

$$\text{bio-Triton@}Ru^{*}\text{Nps} \rightarrow \text{bio-Triton@RuNps} + h\nu \quad (5)$$

where TPrA tri-*n*-propylamine; bio-Triton@RuNps is the $[Ru(bpy)_3]^{2+}$; bio-Triton@Ru^{-}Nps is the $[Ru(bpy)_3]^{+}$; bio-Triton@Ru*Nps is the $[Ru(bpy)_3]^{2+}$* embedded in the nanoparticle and P1 is the product of the homogeneous $TPrA^{\bullet}$ oxidation.

It can be clearly seen that bio-Triton@RuNPs show a much higher ECL intensity than bio-Igepal@RuNps. This difference can be only in part explained by the higher doping degree observed for the NPs synthesized with the Triton surfactant. In fact, even after normalizing the ECL intensity by the number of dyes/NP, bio-Triton@RuNP still displays a higher intensity (see Table S2), thus suggesting that other factors, e.g., the different ζ-potentials and photoluminescence quantum yields, should be considered. The positive ζ-potential of bio-Igepal@RuNP is, according to previous results,[38] disadvantageous to the ECL emission, most probably because of the electrostatic repulsion between the NP surface and the approaching co-reactant cationic intermediates. For this problem, the ECL generation with NPs so far was resctricted to the use of hydrophilic co-reactants (such as 2-(dibutylamino)ethanol), thus barring the efficient ECL generation achievable with TPrA[33][38]. However, our data show that we were able with this synthetic strategy to obtain NPs endowed with the correct NPs parameters (e.g. ζ-potentials, biorecognition unit, hydrophobicity, dye distribution and NP size) for an efficient ECL generation using TPrA (see figure S3).
The enhanced ECL intensity obtained with low concentrations of bio-Triton@RuNPs and the use of TPrA as co-reactant prompted us to test such NPs in ECL imaging, which was unsuccessful with other core-shell NPs likely due to the above detrimental effects. According to the mechanism schematized in Figure 3B (see also equation 1-5), ECL imaging was performed on single 2.8 µm beads functionalized with either bio-Triton@RuNps (beads@Triton) or a biotinylated antibody labelled with $[Ru(bpy)_3]^{2+}$ complex (beads@bio-Ru), mimicking the analytical approach of commercial ECL-based immunoassay system (see SI for the beads functionalization and confocal characterization, Figure S4). Interestingly, the ECL intensity obtained in case of beads@Triton was 8.5-fold higher (see Figures 3C, D, table S4), representing a very interesting and promising result.
ECL images from 2.8 µm beads functionalized (figure 3C and 3D), from multiple beads (Figure S5-7) and respective ECL emission profiles (Figure 3E), confirm the massive ECL signal enhancement of beads@Triton (grey line) compared to beads@bio-Ru, (black line and see the inset of figure 3E). To quantitively compare the two cases, the amount of Ru immobilised onto the surface of the microbeads was quantified by ICP-MS analysis (table S3). As it can be seen, the dye concentration was about 660 times higher in the case of beads@Triton, a value that is in line with an expected similar occupancy of the active sites onto the microbead surface by either the biotinylated Ru-derivatized anibody or bio-Triton@RuNps, which contain 6[43] and 4800 $[Ru(bpy)_3]^{2+}$complexes, respectively. This means that only a small portion of the Ru complexes (around 1.3%, assuming a yes-or-not system) participate to the vast (750%) increase of ECL emission with respect to the commercially available approach.

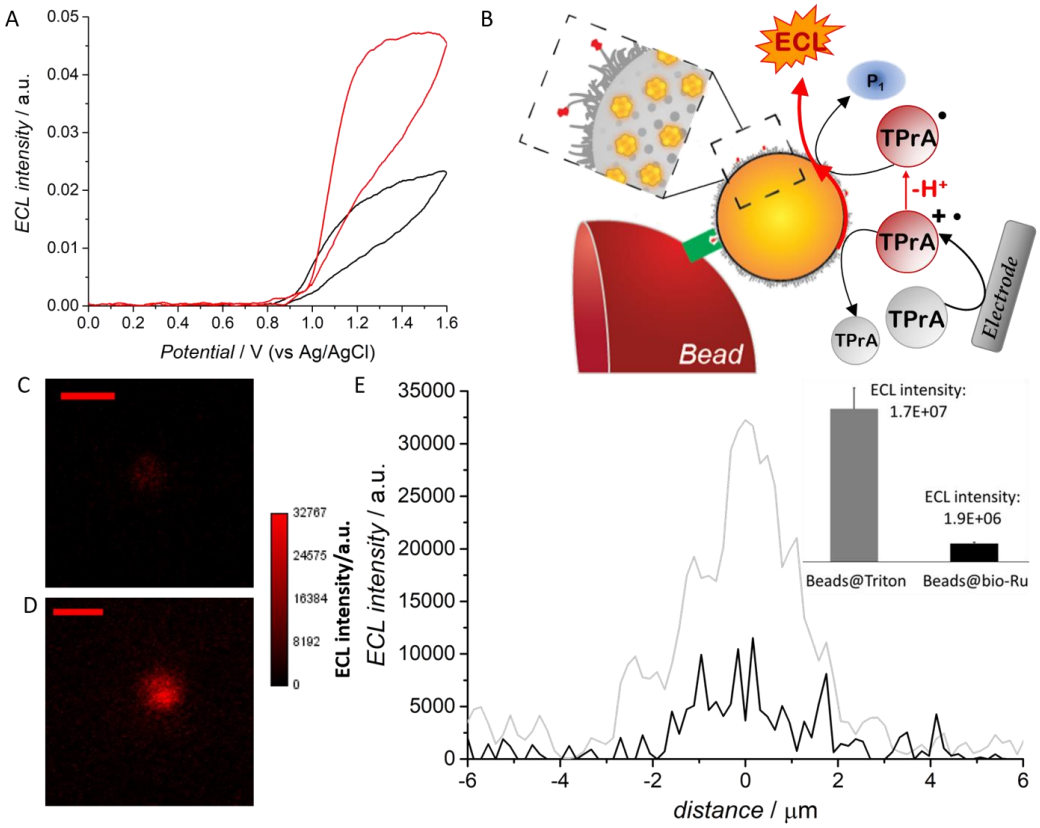

Figure 3. (A) ECL intensity potential curves in the presence of TPrA 180mM in a 1nM solution of bio-Igepal@RuNp (black line) and of bio-Triton@RuNp (red line). Cyclic voltammetries with voltage scanned between 0 V and +1.6 V, scan rate 0.1 V s^{-1}. Glassy Carbon electrode referred to Ag/AgCl. Pt spiral as counter electrode. PMT bias 750V. (B) The heterogeneous mechanism for the "oxidative-reduction" co-reactant ECL generation obtained using 2.8 µm beads labelled with bio-Triton@RuNp (yellow sphere) through a streptavidin (green tool)-biotin (red tool) bond. Tri-*n*-propylamine (TPrA) is oxidized at the electrode, generating the radical cation ($TPrA^{+\bullet}$), which deprotonates, forming the radical ($TPrA^{\bullet}$). The radical and radical cation react with the ECL luminophore $[Ru(bpy)_3]^{2+}$ (yellow square), inside the bio-Triton@RuNp located on magnetic beads (red semi-sphere). (C) Electrochemiluminescence (ECL) imaging of 2.8 µm single bead labelled with biotinylated $[Ru(bpy)_3]^{2+}$complex (beads@bio-Ru) and (D) with bio-Triton@RuNp (beads@Triton). They were obtained by applying a constant potential of 1.4 V (vs. Ag/AgCl) for 4 s in 180 mM TPrA and 0.2 M phosphate buffer (PB). Pt wire as counter electrode. EMCCD camera coupled with a potentiostat. Integration time, 8 s; magnification, X100; Scale bar, 5 µm. (E) Comparison of the beads profile lines (black line, Beads@bio-Ru; grey line, Beads@Triton). Inset of the comparison between integrated intensity values calculated for Beads@bio-Ru (black) and Beads@Triton (grey), error ar shows the standard deviation (n =9).

This result, already very promising *in se*, suggests that, acting on the synthetic procedure can lead to an even more pronounced signal increase. Further investigation in this direction will be performed for implementing the combination between NPs and the ECL imaging. In addition, the ECL from beads@Triton showed improved stability compared with beads@bio-Ru (Figure S8 and supplementary movie S1) thanks to the nano-enviroment of silica matrix that protect against undesired electrochemical reactions, increasing even more their potential performance. In the present case, even bio-Ru dyes show a longer lifetime compared to the $[Ru(bpy)_3]^{2+}$ complex in water, nearly as long as $[Ru(bpy)_3]^{2+}$ in Triton NPs (FLIM images in Fig. S4, Table S4). Owing to this partial shielding effect, the enhanced stability could be even larger if compared with molecular ECL dyes fully exposed to oxygen.

To conclude, we synthesized a new family of silica NPs, named bio-Triton@RuNps, obtained following the reverse microemulsion method and derivatized with biotin. Using this synthetic approach, oppositely to what observed with another kind of NPs, [33,38] the high dye doping degree (ca 4800 complexes every NP) did not bring to a positive surface charge thus allowing a high ECL emission. Moreover, by using TPrA as coreactant, these DDSNPs lead to a remarkable enhancement of ECL signal compared to the conditions mimicking the commercial ECL-based immunoassay system (i.e., based on an antibody labelled with 6 dyes). Moreover, the silica matrix is able to increase the stability of the ECL signal, increasing even more the potential performances of these NPs. These results support the application of such NPs in ECL microscopy techniques and also opens a new promising path towards more sensitive analyte detection, even in biosensing and in point-of-care devices. The improvement the the number of complexes active in the generation of higher ECL signals and an even larger increase in the ECL stability represent a further push to steer possible impactful investigations in this direction.

Acknowledgements
This work is supported by the Italian Ministero dell'Istruzione, Università e Ricerca (2017EKCS35, PRIN-2017FJCPEX, PRIN-2017PBXPN4), University of Bologna. The authors are grateful to Dr. Daniela Manzini (CIGS of Modena "Centro Interdipartimentale Grandi Strumenti") for ICP-MS analysis.

Keywords: dye-doped silica nanoparticles • electrochemiluminescence • electrochemistry • nanomaterials • ECL imaging

References

[1] N. Sojic, *Analytical Electrogenerated Chemiluminescence: From Fundamentals to Bioassays. Detection Science.*, Royal Society Of Chemistry (RSC) Publishing, **2020**.
[2] M. Hesari, Z. Ding, *J. Electrochem. Soc.* **2016**, *163*, H3116–H3131.
[3] M. M. Richter, *Chem. Rev.* **2004**, *104*, 3003–3036.
[4] A. Zanut, Andrea Fiorani, S. Canola, T. Saito, N. Ziebart, S. Rapino, S. Rebeccani, A. Barbon, T. Irie, H.-P. Josel, et al., *Nat. Commun.* **2020**, 10.1038/s41467-020-16476–2.
[5] Y. Cao, X. Gou, J. Zhu, *Anal. Chem.* **2020**, *92*, 431−454.
[6] R. Forster, P. Bertoncello, T. Keyes, *Annu Rev. of Anal. Chem.* **2009**, *2*, 359–385.
[7] S. R. Chinnadayyala, J. Park, H. Thi, N. Le, M. Santhosh, *Biosens. Bioelectron.* **2019**, *126*, 68–81.
[8] Irkham, A. Fiorani, G. Valenti, N. Kamoshida, F. Paolucci, Y. Einaga, *J. Am. Chem. Soc.* **2020**, *142*, 1518–1525.
[9] I. Bist, S. Bhakta, D. Jiang, T. E. Keyes, A. Martin, R. J. Forster, J. F. Rusling, *Anal. Chem.* **2017**, 12441–12449.
[10] K. Kadimisetty, I. M. Mosa, S. Malla, J. E. Satterwhite-Warden, T. M. Kuhns, R. C. Faria, N. H. Lee, J. F. Rusling, *Biosens. Bioelectron.* **2016**, *77*, 188–193.
[11] L. Xu, Y. Li, S. Wu, X. Liu, B. Su, *Angew. Chem. Int. Ed.* **2012**, *51*, 8068–8072.
[12] C. Ma, W. Wu, L. Li, S. Wu, J. Zhang, Z. Chen, J. J. Zhu, *Chem. Sci.* **2018**, *9*, 6167–6175.
[13] A. Zanut, A. Fiorani, S. Rebeccani, S. Kesarkar, G. Valenti, *Anal. Bioanal. Chem.* **2019**, *411*, 4375–4382.
[14] G. Valenti, S. Scarabino, B. Goudeau, A. Lesch, M. Jović, E. Villani, M. Sentic, S. Rapino, S. Arbault, F. Paolucci, et al., *J. Am. Chem. Soc.* **2017**, *139*, 16830–16837.
[15] X. Wang, H. Gao, H. Qi, Q. Gao, C. Zhang, **2018**, DOI 10.1021/acs.analchem.7b04359.

[16] J. Zhang, R. Jin, D. Jiang, H. Chen, *J. Am. Chem. Soc.* **2019**, *141*, 10294–10299.
[17] H. Ding, W. Guo, B. Su, *Angew. Chem. Int. Ed.* **2020**, 449–456.
[18] S. Voci, B. Goudeau, G. Valenti, A. Lesch, M. Jović, S. Rapino, F. Paolucci, S. Arbault, N. Sojic, *Journal of the American Chemical Society* **2018**, *140*, 14753–14760.
[19] M. Sentic, M. Milutinovic, F. Kanoufi, D. Manojlovic, S. Arbault, N. Sojic, *Chem. Sci* **2014**, *5*, 2568–2572.
[20] W. Miao, J.-P. Choi, A. J. Bard, *J. Am. Chem. Soc.* **2002**, *124*, 14478–14485.
[21] J. K. Leland, *J. Electrochem. Soc.* **1990**, *137*, 3127.
[22] Y. Zu, A. J. Bard, *Anal Chem* **2000**, *72*, 3223–3232.
[23] W. Miao, *Chem. Rev.* **2008**, 2506–2553.
[24] "Roche Diagnostic corporation, www.roche.com," **2018**.
[25] "The Meso Scale Discovery, www.mesoscale.com/en/technical_resources/our_technology/multi-array," **2018**.
[26] G. Valenti, E. Rampazzo, S. Kesarkar, D. Genovese, A. Fiorani, A. Zanut, F. Palomba, M. Marcaccio, F. Paolucci, L. Prodi, *Coord. Chem. Rev.* **2018**, *367*, 65–81.
[27] Z. Farka, T. Juřík, D. Kovář, L. Trnková, P. Skládal, *Chem. Rev.* **2017**, *117*, 9973–10042.
[28] S. Brakmann, *Angew. Chem. Int. Ed.* **2004**, *43*, 5730–5734.
[29] S. Kesarkar, E. Rampazzo, A. Zanut, F. Palomba, M. Marcaccio, G. Valenti, L. Prodi, F. Paolucci, *Curr. Opin. Electrochem.* **2018**, *7*, 130–137.
[30] P. Bertoncello, P. Ugo, *ChemElectroChem* **2017**, *4*, 1663–1676.
[31] S. Carrara, F. Arcudi, M. Prato, L. De Cola, *Angew. Chem. Int. Ed.* **2017**, *56*, 4757–4761.
[32] K. Imai, G. Valenti, E. Villani, S. Rapino, E. Rampazzo, M. Marcaccio, L. Prodi, F. Paolucci, *J. Phys. Chem. C* **2015**, *119*, 26111–26118.
[33] G. Valenti, E. Rampazzo, S. Bonacchi, L. Petrizza, M. Marcaccio, M. Montalti, L. Prodi, F. Paolucci, *Journal of the American Chemical Society* **2016**, *138*, 15935–15942.
[34] X. Chen, Y. Liu, Q. Ma, *J. Mat. Chem. C* **2018**, *6*, 942–959.
[35] B. Lora, C. Jai-Pil, *ChemElectroChem* **2017**, *4*, 1573–1586.
[36] M. Montalti, L. Prodi, E. Rampazzo, N. Zaccheroni, *Chem. Coord. Rev.* **2014**, *43*, 4243–4268.
[37] W. Arap, R. Pasqualini, M. Montalti, L. Petrizza, L. Prodi, E. Rampazzo, N. Zaccheroni, S. Marchiò, *Curr. Med. Chem.* **2013**, *20*, 2195–2211.
[38] S. Kesarkar, S. Valente, A. Zanut, F. Palomba, A. Fiorani, M. Marcaccio, E. Rampazzo, G. Valenti, F. Paolucci, L. Prodi, *J. Phys. Chem. C* **2019**, *123*, 5686–5691.
[39] G. Valenti, E. Rampazzo, S. Bonacchi, L. Petrizza, M. Marcaccio, M. Montalti, L. Prodi, F. Paolucci, *J. Am. Chem. Soc.* **2016**, *138*, 15935–15942.
[40] L. Qi, *Science* **2006**, 6183–6207.
[41] C.-L. Chang, H. S. Fogler, *Langmuir* **1997**, *13*, 3295–3307.
[42] B. Del Secco, L. Ravotto, T. V Esipova, S. A. Vinogradov, D. Genovese, N. Zaccheroni, E. Rampazzo, L. Prodi, *Photochem. Photobiol. Sci.* **2019**, *18*, 2142–2149.
[43] *Biotinilated Antibody Labelled Ru(Bpy)32+ Where Used for Increase the Number of Dye for Active Site with an Averege of 6 Dye for Microbeads Active Site.*